Materials Advances

ROYAL SOCIETY OF CHEMISTRY

PAPER

View Article Online
View Journal | View Issue

Cite this: *Mater. Adv.*, 2023, 4, 5564

Ionic self-assembly of pillar[5]arenes: proton-conductive liquid crystals and aqueous nanoobjects with encapsulation properties†

Iván Marín,[ab] Rosa I. Merino,[ac] Joaquín Barberá,[ab] Alberto Concellón[ab] and José L. Serrano *[ab]

Received 12th September 2023,
Accepted 10th October 2023

DOI: 10.1039/d3ma00698k

rsc.li/materials-advances

Liquid crystal (LC) pillar[*n*]arenes have been barely explored due to their time-consuming and complicated synthesis, despite their promising properties for metal-ion separation, drug delivery, or surface functionalization. Herein, we report an easy and reliable method to functionalize pillar[*n*]arene macrocycles through electrostatic interactions. These ionic materials were prepared by ionically functionalizing a pillar[*n*]arene containing ten amine terminal groups with six different carboxylic acids. This supramolecular approach results in ionic pillar[*n*]arenes which self-organize into LC phases with good proton-conducting properties. Moreover, ionic functionalization provides a new amphiphilic character to the pillar[*n*]arenes, which self-assemble in water to produce a variety of nanoobjects (*i.e.*, spherical or cylindrical micelles, vesicles, solid nanospheres, or nanotubes) that are capable of encapsulating a model hydrophobic drug. Interestingly, the presence of coumarin moieties in the chemical structure of the ionic pillar[*n*]arenes results in self-organized materials with light-responsive properties due to the ability of coumarins to undergo photo-induced [2+2] cycloaddition. In particular, we demonstrate that coumarin pohotodimerization can be employed to fabricate mechanically stable proton-conductive LC materials, as well as to obtain photo-responsive nanocarriers with light-induced release of encapsulated molecules.

Introduction

Liquid crystal (LC) macrocycles are a prominent class of LCs wherein the shape-persistent cavity and the rich host–guest properties of the macrocyclic unit in an ordered environment enable a plethora of opportunities in the design of functional materials.[1,2] Several macrocycles have been employed for the preparation of LCs, including calixarenes, oligopeptides, phenylacetylenes, or cycloaramides, among others.[3–5] Nonetheless, the use of pillar[*n*]arene derivatives has been less often considered, despite their promising properties in metal-ion separations,[6] drug delivery,[7] surface modifications,[8] or the preparation of supramolecular polymers.[9] LC pillar[*n*]arenes are usually synthesized by the functionalization of a central macrocyclic scaffold with promesogenic units, resulting in lamellar and columnar LC organizations.[10,11] Additionally, pillar[*n*]arene macrocycles have been decorated with azobenzene or coumarin moieties to yield LCs that showed photoactive and/or fluorescent properties.[12–14] The introduction of such complex, function-bearing units into pillar[*n*]arenes requires the use of extremely efficient reactions, such as "click" chemistry. However, to avoid the time-consuming synthesis associated with the preparation of these covalent systems, we envisioned that a very interesting approach may consist of using supramolecular interactions to functionalize pillar[*n*]arene macrocycles. Among the diverse non-covalent interactions that hold molecular building blocks together, electrostatic interactions have recently shown high potential to create LCs with promising properties as ion-conductors or drug delivery systems.[15–17] In these ionic materials, the presence of charged sites within the molecular structure results in a cooperative assembly process that leads to self-organized nanostructures both in solution and in solid state. The most representative example are ionic dendrimers that are capable of self-organizing in the bulk to produce LC behavior even without being functionalized with any promesogenic unit.[18,19] Ionic interactions are essential in this self-assembly process as the segregation between polar and apolar parts is the driving force for the formation of the LC phases. Similarly, the introduction of charged sites within a dendritic polymer modifies its amphiphilic character and results in a microphase separation in solution that leads to the formation of several self-assembled nanoobjetcs (*e.g.*, spherical or cylindrical micelles, vesicles, nanotubes...).[20–22]

[a] *Instituto de Nanociencia y Materiales de Aragón (INMA), CSIC-Universidad de Zaragoza, 50009 Zaragoza, Spain. E-mail: joseluis@unizar.es*
[b] *Departamento de Química Orgánica, Facultad de Ciencias, Universidad de Zaragoza, 50009 Zaragoza, Spain*
[c] *Departamento de Física de la Materia Condensada, Facultad de Ciencias, Universidad de Zaragoza, 50009 Zaragoza, Spain*

† Electronic supplementary information (ESI) available. See DOI: https://doi.org/10.1039/d3ma00698k

Herein, we report for the first time the use of ionic non-covalent interactions to functionalize a pillar[*n*]arene macrocycle. This approach results in a new family of ionic pillar[5]arenes with unprecedented functional properties. In particular, we prepared ionic complexes between the terminal amine groups of a pillar[5]arene (**P5N10**) and several carboxylic acids (Fig. 1). Formation of ionic pairs leads to a hierarchical self-assembly process, in which the charged sites promote additional self-assembly that ultimately results in the formation of wide variety of nanostructured materials. In the solid state, the ionic pillar[5]arenes self-organized into LC phases with good proton-conducting properties; the ionic segregated areas (formed by the ionic salts) are the continuous ionic pathways necessary for proton transport. The same interactions that occurred in the solid state also appeared in aqueous solution, and these ionic pillar[5]arene self-organized in a large variety of assemblies, such as spherical or cylindrical micelles, vesicles, solid nanospheres, or nanotubes. Additionally, we introduced coumarin units in the chemical structure of some of our ionic pillar[5]arenes, and thus the resulting nanostructured materials displayed light-responsive properties due to the ability of coumarins to undergo photo-induced [2+2] cycloaddition.[23,24] Specifically, LC phases were crosslinked to lock the LC arrangement and fabricate mechanical stable proton-conductive materials. In the case of the aqueous self-assemblies, coumarin units allowed obtaining photo-responsive nanocarriers that showed light-induced release of guest molecules.

Results and discussion

Preparation of ionic compounds

The synthesis of the acids (**AcC$_{11}$**, **AcBzC$_{11}$**, **Acd$_1$C$_{11}$**, **AcC$_{11}$Cou**, **AcBzC$_{11}$Cou**, and **Acd$_1$C$_{11}$Cou**) and the pillar[5]arene **P5N10** was carried out following previously reported methods.[25–28] All ionic compounds were prepared by the same procedure: a THF solution of the corresponding acid was slowly added to a THF solution of pillar[5]arene **P5N10** in a 10 : 1 stoichiometry to completely functionalize all the amine groups of **P5N10**. The mixture was ultrasonicated for 5 min, then THF was slowly evaporated at room temperature, and the sample was dried under vacuum at 40 °C until the weight remained constant. Formation of the complexes between **P5N10** and the different acids was confirmed by infrared spectroscopy (IR) and nuclear magnetic resonance (NMR).

As an example, the IR spectra of **Acd$_1$C$_{11}$Cou**, **Acd$_1$C$_{11}$Cou-P5N10** and **P5N10** are shown in the Fig. 2. In the C=O region, **Acd$_1$C$_{11}$Cou** showed two stretching bands at 1733 and 1676 cm^{-1} that correspond to the ester groups of the coumarin moieties and to the dimeric form of the carboxylic acid, respectively. However, in the IR spectrum of **Acd$_1$C$_{11}$Cou-P5N10**, the dimeric band of the acid was replaced by two bands at 1555 and 1369 cm^{-1} due to asymmetric and symmetric stretching vibrations of the newly formed carboxylate groups, thereby indicating the formation of the ionic complex.

The NMR spectra of the ionic complexes also confirmed the formation of the ionic salts. As an example, Fig. 3b displays the ^{1}H NMR spectra of **AcBzC$_{11}$Cou**, **P5N10** and **AcBzC$_{11}$Cou-P5N10**, in which the broad signal at 12.53 ppm of the carboxylic acid proton of **AcBzC$_{11}$Cou** disappeared in the spectrum of the ionic complex **AcBzC$_{11}$Cou-P5N10**. Moreover, the protons H_a and H_b of the methylene groups of **P5N10** shifted from 3.81/2.91 to 3.91/3.30 ppm, respectively. The ^{13}C NMR spectra also showed the ionic salt formation. For instance, the carboxylic acid carbon signal shifted from 167.00 to 167.94 ppm due to the formation of the carboxylate (Fig. 3c). The carbon adjacent to the carboxylic acid group shifted from 122.76 to 125.20 ppm, also evidencing the ionic complex formation (Fig. S11, ESI†).

^{1}H–^{1}H NOESY experiments (Fig. S14, ESI†) were recorded to fully confirm the formation of the ionic salts. NOESY experiments

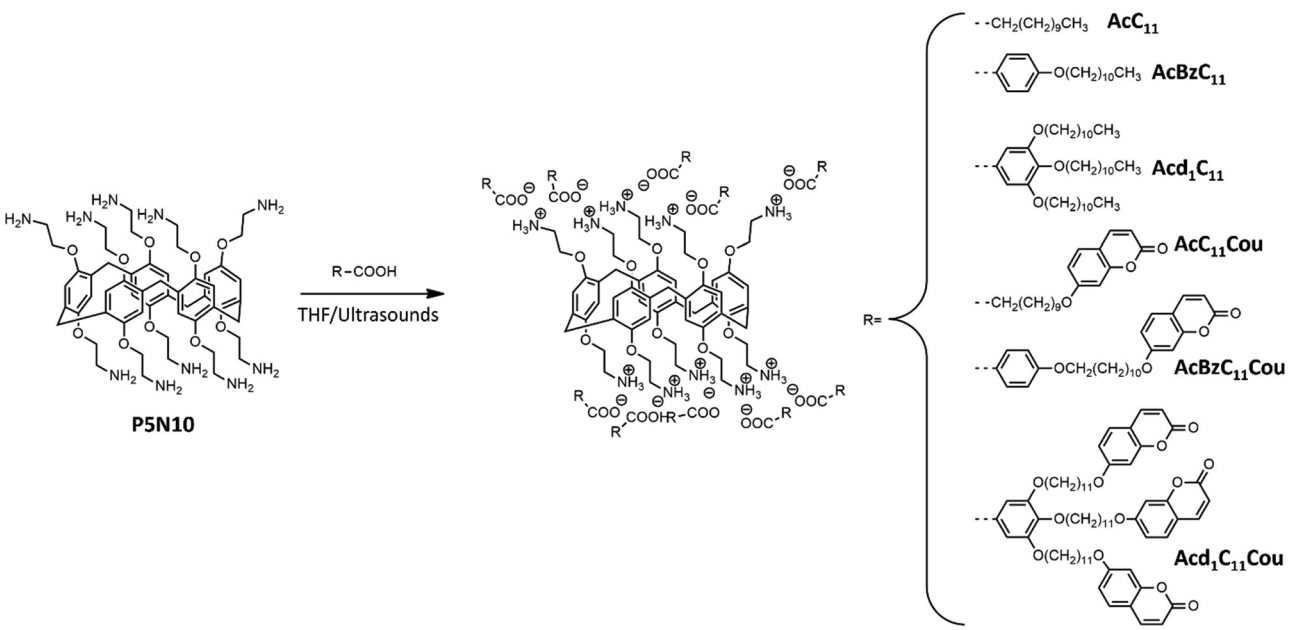

Fig. 1 Scheme of the preparation of the six ionic complexes studied.

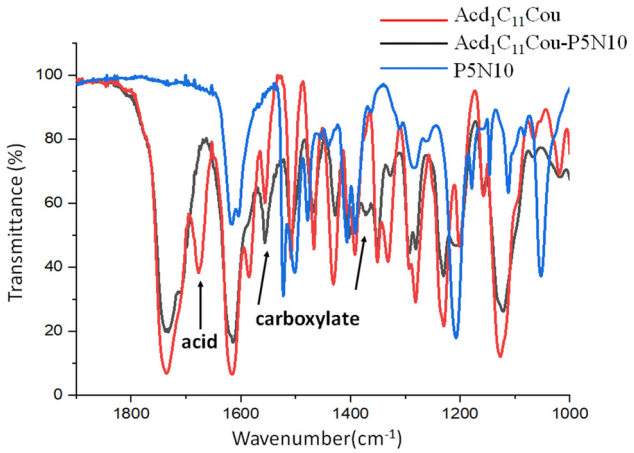

Fig. 2 FTIR spectra (C═O *st.* region). (See Fig. S18 for the FTIR spectra in the complete frequency range, ESI†).

are widely used in supramolecular chemistry as they provide information about the spatial relationships (distance) between molecules.[29] In this case, meaningful correlations were observed between the signal H_b of **P5N10** and the signal H_f of **AcBzC$_{11}$Cou**, thereby indicating their proximity in the space because of the ionic bond formation.

Liquid crystalline properties

Thermal stability is required for melt processing and was studied by thermogravimetric analysis (TGA). All ionic complexes showed good thermal stability with 2% weight loss temperatures ($T_{2\%}$) above the isotropization temperatures (Table 1).

The thermal and liquid crystal properties were studied by polarized-light optical microscopy (POM), differential scanning calorimetry (DSC), and X-ray diffraction (XRD), and the results

Table 1 Thermal properties of ionic compounds

Compound	$T_{2\%}$ (°C)[a]	Thermal transitions[b]
AcC$_{11}$-P5N10	166	Cr 142 I
AcBzC$_{11}$-P5N10	200	N$_g$ 108 N 161 I
Acd$_1$C$_{11}$-P5N10	224	N 120[c] I
AcC$_{11}$Cou-P5N10	135	Cr 97 I
AcBzC$_{11}$Cou-P5N10	135	N$_g$ 44 N 116 I
Acd$_1$C$_{11}$Cou-P5N10	226	N$_g$ 25 N 69 I

[a] Temperature at which 2% of mass lost is detected in the TGA curve. [b] DSC data of the 2nd heating scan at a rate of 10 °C min^{-1}. Ng: glassy nematic phase, N: nematic phase, Cr: crystal, I: isotropic liquid. [c] POM data.

are summarized in Table 1. **AcC$_{11}$-P5N10** and **AcC$_{11}$Cou-P5N10** are crystalline materials that melt to give an isotropic liquid phase. Nonetheless, the introduction of benzoic acids into **P5N10** *via* ionic interactions led to ionic complexes that showed stable enantiotropic liquid crystal phases over a wide temperature range. Ionic complexes containing coumarin units (*i.e.*, **AcBzC$_{11}$-Cou-P5N10** and **Acd$_1$C$_{11}$Cou-P5N10**) exhibited lower isotropization temperatures than those of ionic complexes containing undecyl alkyl chains without terminal coumarin moieties (*i.e.*, **AcBzC$_{11}$-P5N10** and **Acd$_1$C$_{11}$-P5N10**). While highly birefringent textures were observed by POM in **AcBzC$_{11}$-P5N10** and **Acd$_1$C$_{11}$-P5N10**, **AcBzC$_{11}$Cou-P5N10** and **Acd$_1$C$_{11}$Cou-P5N10** showed spontaneous tendency to homeotropic alignment and the mesophase was observed *via* POM on applying mechanical stress to the samples (Fig. 4b). This spontaneous homeotropic alignment is induced by terminal coumarin units, which are known to produce such phenomenon in other liquid crystals containing coumarins.[27]

The assignment of the mesophase was achieved by XRD. The XRD patterns showed diffuse scattering in the low-angle region, whereas a broad diffuse scattering maximum was observed in

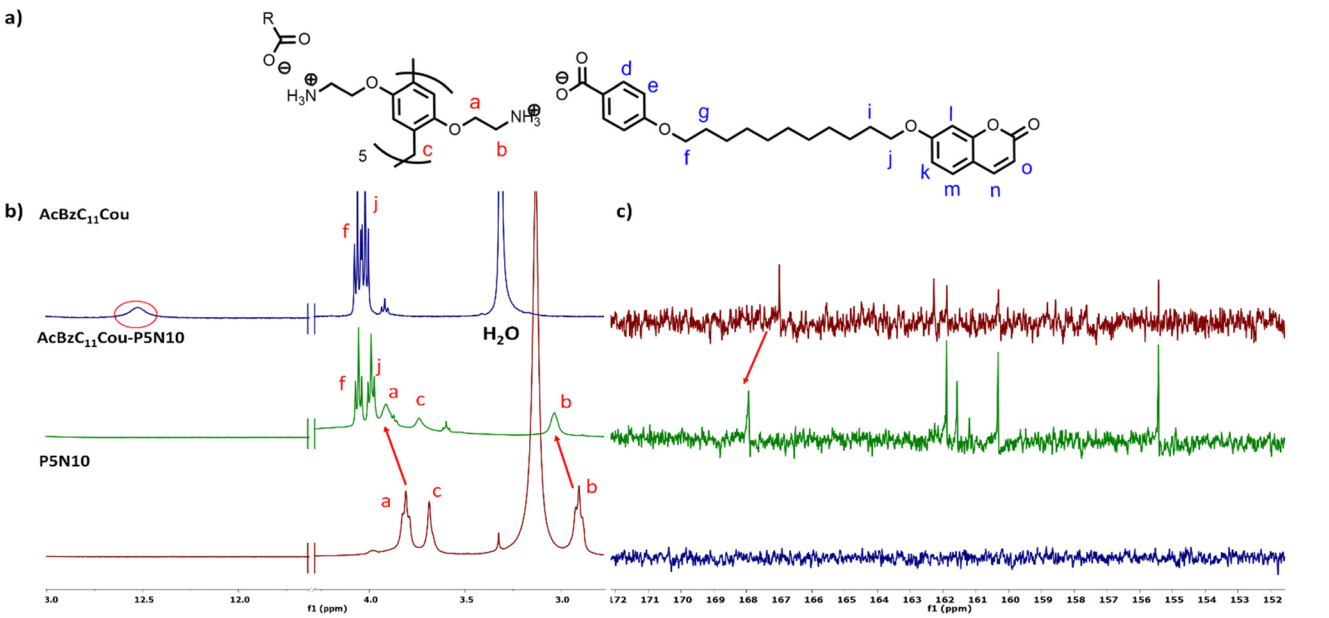

Fig. 3 (a) Schematic representation of **AcBzC$_{11}$Cou-P5N10**, (b) ^{1}H NMR and (c) ^{13}C NMR comparative of **AcBzC$_{11}$Cou-P5N10**, **AcBzC$_{11}$Cou** and **P5N10**.

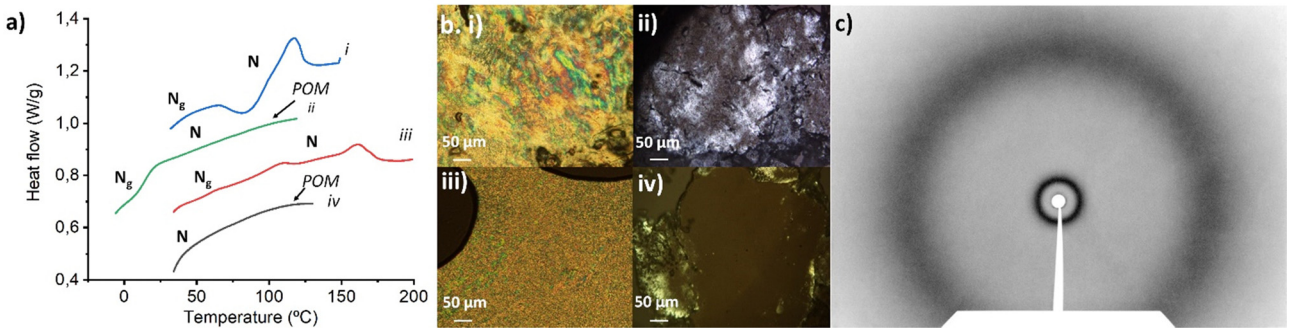

Fig. 4 (a) DSC curves in the second heating of (i) **AcBzC$_{11}$Cou-P5N10** (ii) **Acd$_1$C$_{11}$Cou-P5N10**, (iii) **AcBzC$_{11}$-P5N10** and (iv) **Acd$_1$C$_{11}$-P5N10** (b) POM textures of (i) **AcBzC$_{11}$Cou-P5N10** (ii) **Acd$_1$C$_{11}$Cou-P5N10**, (iii) **AcBzC$_{11}$-P5N10** and (iv) **Acd$_1$C$_{11}$-P5N10** (c) XRD example of **AcBzC$_{11}$Cou-P5N10**.

the high-angle region that is related to the lateral interactions of the hydrocarbon chains (Fig. 4c). The absence of Bragg reflections and the presence of only diffuse scattering indicate that there is no periodical order, and thus such XRD patterns are consistent with nematic mesophases that have only orientational order. Although an increase in the number of alkyl substituents in the molecule (from 10 to 30) reduces the transition temperatures (*i.e.*, both T_g and $T_{N\text{-}I}$) (Fig. 4a), it does not significantly modify the type of the mesophase nor alter the degree of order with the nematic phase.

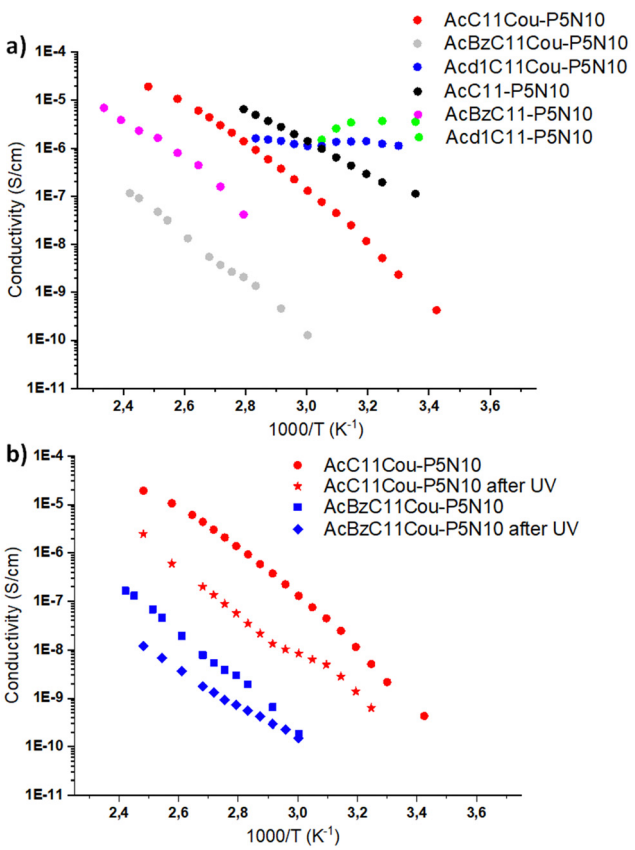

Fig. 5 (a) Conductivity variation with temperature, measured by EIS, of (a) all ionic compounds measured (b) **AcC$_{11}$Cou-P5N10** and **AcBzC$_{11}$Cou-P5N10** before and after irradiation with 325 nm light.

Proton conduction properties

Ionic liquid crystals are promising materials for ion conduction. The presence of ten charged groups in our ionic LC pillar[5]arenes make them ideal materials for proton transport. To measure the proton conduction properties, we used electrochemical impedance spectroscopy (EIS) in samples that consisted of thin films sandwiched between two ITO-coated electrodes using glass spacers of 25 µm. Thin films of the samples were prepared by pressing the ionic pillar[5]arenes between two ITO-coated electrodes at the isotropization temperature. Then, the cell was slowly cool down to room temperature to obtain samples with a uniform homeotropic alignment over large areas. This alignment process is quite relevant since in anisotropic materials, such as LCs, the measured proton conductivity depends on the macroscopic degree of order and the orientation of the LC phase with respect to the electrodes.

Examples of EIS data (in the form of Nyquist plots) are given in ESI,† Fig. S25. **Acd$_1$C$_{11}$Cou-P5N10** and **Acd$_1$C$_{11}$-P5N10** show a slightly depressed arc corresponding to the electrical response of the compound (conductivity and electrical permittivity), without relevant polarization contribution at the electron conducting electrodes at low frequencies. This is a strong hint that these compounds show electronic conduction, which dominates their electrical response. For the other compounds, **AcC$_{11}$-P5N10**, **AcBzC$_{11}$-P5N10**, **AcC$_{11}$Cou-P5N10** and **AcBzC$_{11}$Cou-P5N10**, the Nyquist plots show a spike towards low frequencies, that is at the high values of Z_{real}, with fast increase of the absolute value of Z_{im}. This corresponds to polarization of the electrodes, typical of ion blocking electronic conducting electrodes (such as ITO) on a mainly ionic conducting material. The dominant charge conduction carriers in those samples would be ions. Since diffusible ions other than protons are not present in the ionic LC pillar[5]arenes, the EIS responses were mainly related to proton conduction, which was calculated from the EIS responses and the cell constant. The conductivity was calculated from the value of Z_{real} at the minimum between the spike and the depressed semicircle or form the Z_{real} at low frequencies, as corresponds to each material, and the cell constant.

The conductivity of these materials as a function of the temperature is shown in Fig. 5a. At low temperatures **Acd$_1$C$_{11}$Cou-P5N10** and **Acd$_1$C$_{11}$-P5N10** showed the highest conductivity values

very slightly dependent on temperature and apparently dominated by electronic carriers. We cannot give an explanation to this observation. In contrast, **AcC_{11}Cou-P5N10** and **AcC_{11}-P5N10** showed comparable conductivity values to **Acd_1C_{11}Cou-P5N10** and **Acd_1C_{11}-P5N10** at high temperatures, probably because their crystalline structure favors higher order in these compounds than in nematic mesophases. **AcC_{11}-P5N10** and **$AcBzC_{11}$-P5N10** and their counterparts with coumarin moieties show temperature dependent ionic conductivity that can be ascribed to proton conductivity, with relatively large activation energies from 0.8 eV to 1.4 eV in the measured temperature range. The proton conductivity is higher for **AcC_{11}-P5N10** than for **$AcBzC_{11}$-P5N10** and is smaller in the compounds with coumarin units with respect to the compounds without them. Conformational differences in the LC mesophases must be behind the differences in conductivity and activation energies. Smaller molecules such as **AcC_{11}-P5N10** with crystalline order would favor proton diffusion through shorter effective hopping distances.

The conformational arrangement of the mesophases is expected to contribute strongly to the conductivity. The mobile protons are located at the COO^-/NH_3^+ ionic bonds, around the pillar[5]ene macrocycle. Rod-shaped ionic pillar[5]arenes (*i.e.*, **AcC_{11}Cou-P5N10** and **AcC_{11}-P5N10**), which possess a crystal-ordered phase, show the highest ionic conductivity in the series. **$AcBzC_{11}$Cou-P5N10** and **$AcBzC_{11}$-P5N10**, in which each benzoic ring has one substituent (10 alkyl chains per pillar[5]arene macrocycle) show also an elongated shape (rod shape), with a nematic phase range, less ordered. Their proton conductivity is lower than the ones without the benzoic ring (Fig. 6). In **Acd_1C_{11}Cou-P5N10** and **Acd_1C_{11}-P5N10**, the presence of three substituents in each benzoic ring produces a total of 30 alkyl chains per pillar[5]arene macrocycle, probably resulting in a flatter conformation (disk shape). Such an ordering should make easier the proton hopping as long as the distance between molecules (and the ionic bond regions) are kept short. The presence of 30 times more alkyl chains per pillar[5]arene macrocycle might however be increasing the hopping distance (Fig. 6). Nevertheless, as the measured conductivity in these materials is dominated the electronic carriers, a change in the electronic charge distribution must have been produced.

Coumarin compounds undergo a well-known photoinduced [2+2] cycloaddition (so-called photodimerization) to form stable cyclobutene dimers when they are exposed to light of the appropriate wavelength ($\lambda > 300$ nm) (Fig. 7a). This photodimerization was previously exploited as a crosslinking reaction to fabricate mechanical stable membrane materials with a locked LC organization. As a representative example, in the Fig. 7b, the crosslinking of **Acd_1C_{11}Cou-P5N10** in film of 25 μm is showed. Upon irradiation with 325 nm light, the intensity of the π–π^* band of coumarin showed a remarkable decrease, and this is consistent with photodimerization of coumarin units that produced crosslinked polymer networks that retain the morphology of the LC phase. It is apparent that after crosslinking the conductivity values decreased approximately one order of magnitude due to a decrease in the mobility of ion-transporting moieties (Fig. 5b). Such ion conductivity decrease

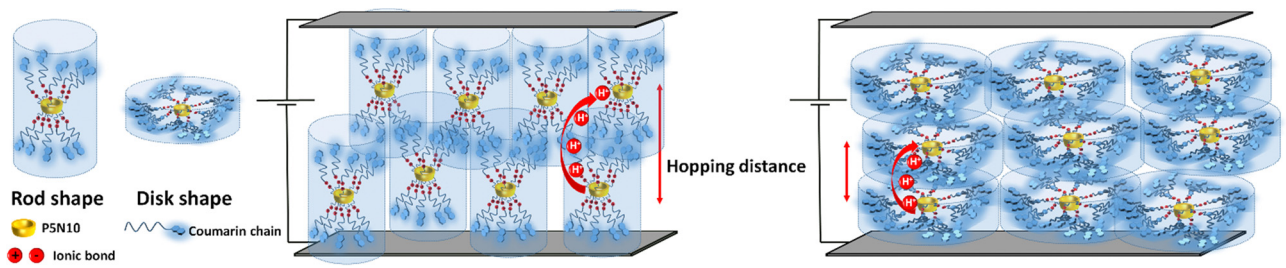

Fig. 6 Schematic representation of rod and disk shape molecules containing coumarins aligned in the ITO-coated electrodes.

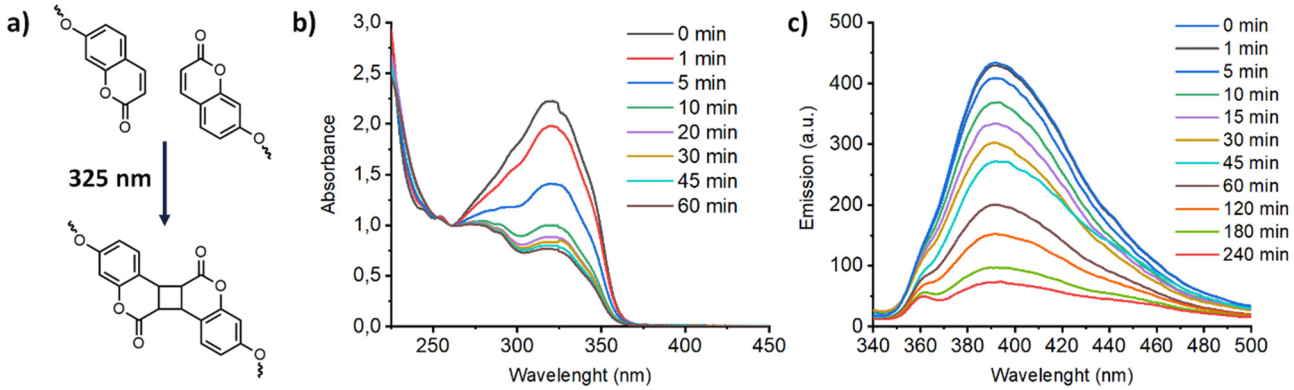

Fig. 7 (a) Photodimerization reaction of coumarins followed by UV (b) and fluorescence (c) in the compound **Acd_1C_{11}Cou-P5N10**.

is similar to those of observed in previously reported polymerizable LCs.[24] Nonetheless, a more dramatic reduction of proton conductivity was observed in **Acd$_1$C$_{11}$Cou-P5N10**, in which no EIS response was observed, suggesting a lack of ion transport in photocrosslinked **Acd$_1$C$_{11}$Cou-P5N10**. This fact can be explained by a total lack of mobility of the ion-transporting moieties (ionic pairs) due to the large number of peripheral photocrosslinkable units (coumarins).

Self-assembly in aqueous solution

Amphiphilic molecules self-assemble in water to yield a variety of well-defined nano-assemblies, such as spherical and tubular micelles or vesicles.[30,31] Formation of these self-assemblies is driven by hydrophobic–hydrophilic interactions, through which the hydrophobic parts of the molecule locate inside of the nano-assembly to minimize their interaction with water, while the hydrophilic segments locate in contact with water to stabilize the nano-assembly. Pillar[*n*]arene derivatives were previously employed to prepare nanoparticles in aqueous solution, wherein the amphiphilic character was obtained by host–guest interactions between an ionic pillar[*n*]arenes and a guest molecule.[32–34] In our case, the introduction of charged sites in the pillar[5]arene scaffold *via* ionic functionalization with carboxylic acids has already modified the amphiphilic character of these macrocycles, which lead to pillar[5]arenes-containing materials with intrinsic amphiphilicity, simplifying the preparation of nano-assemblies. The self-assemblies were prepared by the co-solvent method. Briefly, water was slowly added over a THF solution of the ionic compound (2 mg mL^{-1}) while monitoring the turbidity of the solution. An increase in turbidity indicated that self-assembly process had started. When turbidity kept a stable value, the sample was dialyzed against water to remove the THF, obtaining stable aqueous solutions of self-assemblies. The morphology of the self-assemblies was studied by transmission electron microscopy (TEM) (Fig. 8). **AcC$_{11}$-P5N10** generated solid nanospheres of around 200 nm (Fig. 8a). The introduction of terminal coumarin units in complex **AcC$_{11}$Cou-P5N10** produced a significant variation of the size of the nanospheres, whereas the formation of vesicles was also detected (Fig. 8b). In contrast, ionic complexes derived from benzoic acids produced two clear different morphologies. **AcBzC$_{11}$-P5N10** showed solid ring-shaped structures with a thickness of around 90–120 nm (Fig. 8c), whereas **AcC$_{11}$Bz-Cou-P5N10** produced large tubular nanoaggregates (more than 1 μm in length) incorporating some small vesicles in the walls

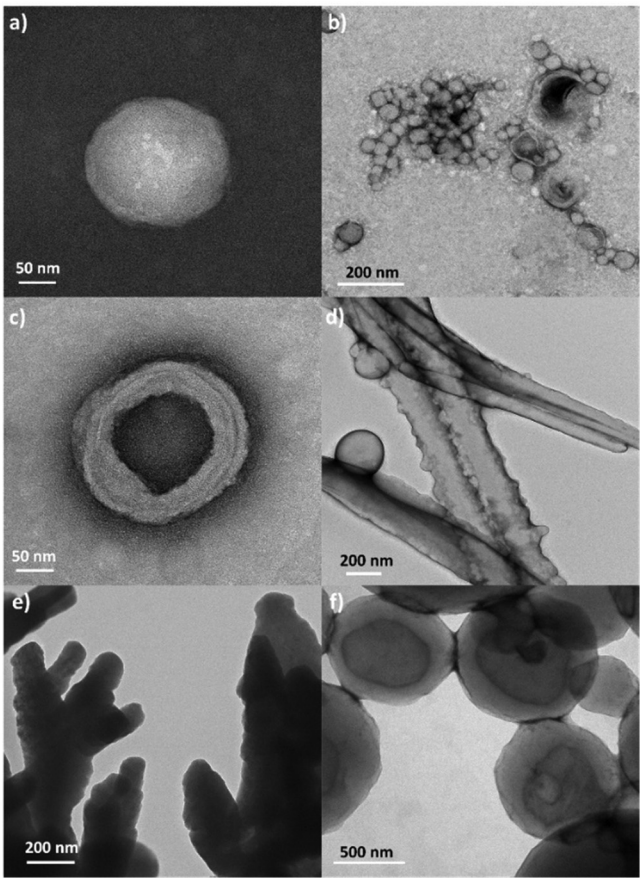

Fig. 8 TEM micrographs of (a) Nanospheres obtained from **AcC$_{11}$-P5N10**, (b) vesicles from **AcC$_{11}$Cou-P5N10** (c) ring-shaped structures from **AcBzC$_{11}$-P5N10** (d) tubular structures from **AcBzC$_{11}$Cou-P5N10** (e) coral shaped structures from **Acd$_1$C$_{11}$P5N10** and (f) vesicles from **Acd$_1$C$_{11}$Cou-P5N10**.

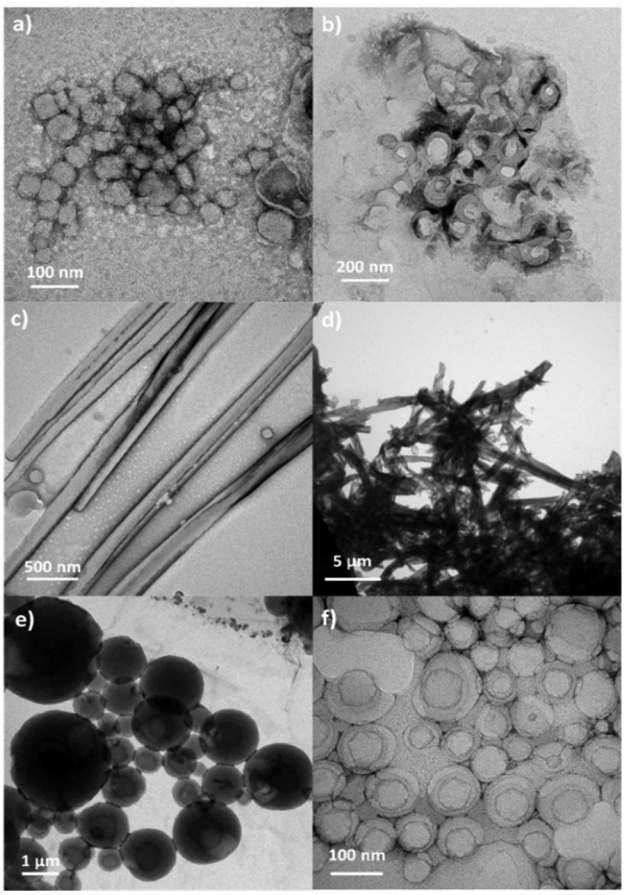

Fig. 9 TEM micrographs of the nanostructures before (left) and after (right) photodimerization: (a) and (b) **AcC$_{11}$Cou-P5N10**, (c) and (d) **AcBzC$_{11}$Cou-P5N10** and (e) and (f) **Acd$_1$C$_{11}$Cou-P5N10**.

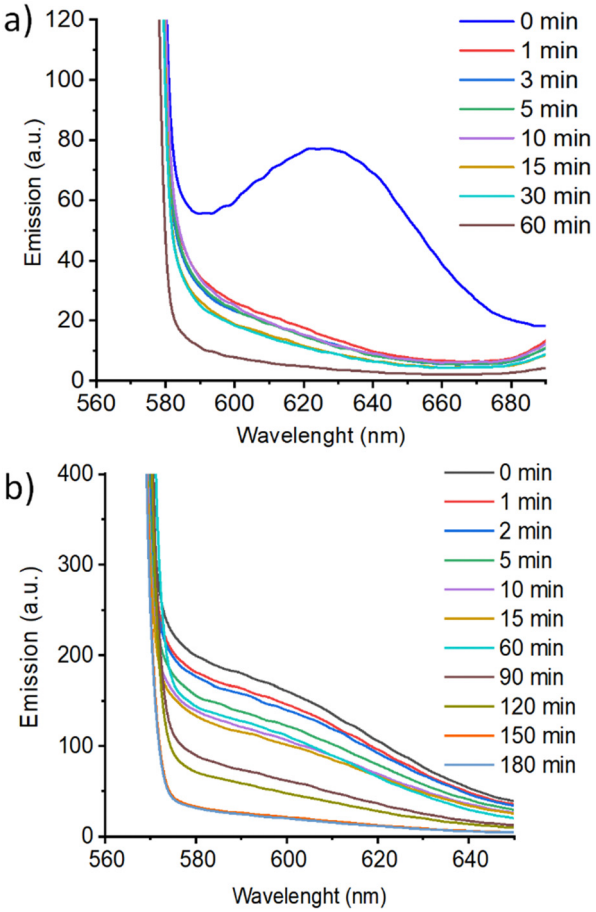

Fig. 10 Delivery of Nile Red in (a) AcC_{11}Cou-P5N10 and (b) Acd_1C_{11}-Cou-P5N10.

of the nanotubes (Fig. 8d). In the case of gallic acid derivatives, **Acd_1C_{11}-P5N10** self-assembled in solid coral-type structures (Fig. 8e), whereas **Acd_1C_{11}Cou-P5N10** that incorporates terminal coumarin moieties exclusively formed large vesicles (>500 nm) (Fig. 8f).

As can be deduced from TEM studies, ionic complexes that incorporate terminal alkyl chains (**AcC_{11}-P5N10**, **$AcBzC_{11}$-P5N10**, and **Acd_1C_{11}-P5N10**) tended to self-assemble into solid nanostructures and the formation of hollow nanostructures (*e.g.*, vesicles or nanotubes) seems to be unfavorable. However, ionic complexes containing terminal coumarin units (**AcC_{11}Cou-P5N10**, **$AcBzC_{11}$Cou-P5N10**, and **Acd_1C_{11}Cou-P5N10**) led to the formation of bilayer-based nano-assemblies, such as vesicles or nanotubes. The presence of terminal coumarin groups may increase the lateral π–π intermolecular interactions favoring the formation of stable bilayers that curve to generate vesicles (**AcC_{11}Cou-P5N10** and **Acd_1C_{11}Cou-P5N10**), or that bend to form tubular structures (**$AcBzC_{11}$Cou-P5N10**).

Additionally, coumarin photodimerization may provide both a type of light-responsive nanocarriers or a facile method to produce cross-linked self-assemblies with enhanced robustness and stability.[35,36] Therefore, we irradiated the corresponding aqueous solutions of the self-assemblies with 325 nm light for one hour. The photodimerization process was monitored by measuring the emission of the solutions. Irradiation with 325 nm light resulted in a gradual decrease of the coumarin emission band at *ca.* 400 nm (Fig. 7c). This photodimerization gave different morphology responses for each nano-assemblies based on coumarin-containing ionic complexes (Fig. 9). Both **AcC_{11}Cou-P5N10** and **$AcBzC_{11}$Cou-P5N10** collapsed, obtaining broken micelles with a non-defined structure (Fig. 9b) or a solid precipitate (Fig. 9d), respectively. Nonetheless, **Acd_1C_{11}Cou-P5N10** yielded stable vesicles after light irradiation, but a significant size reduction was observed in comparison to the vesicles before irradiation (Fig. 9e and f).

Encapsulation and light-induced release of fluorescence probes

These pillar[5]arene-based nano-assemblies may have potential as drug delivery systems, and thus we studied their ability to encapsulate hydrophobic drugs. To test the potential of these self-assemblies as light-responsive nanocarriers, we studied the encapsulation and subsequent release of a fluorescent probe. We selected Nile Red (NR) as a model hydrophobic drug that in a hydrophobic environment presents a fluorescence emission band at 620 nm, but its emission is quenched in hydrophilic environments.[37]

AcC_{11}Cou-P5N10 and **Acd_1C_{11}Cou-P5N10** (2 mg mL^{-1}) self-assemblies were loaded with NR (1.0×10^{-6} M) by stirring overnight the aqueous solutions of the self-assemblies together with NR (diffusion method see ESI† for further details). Encapsulation of NR was confirmed by measuring the emission of the NR-loaded self-assemblies, which showed a strong emission band from 560 to 700 nm ($\lambda_{excitation}$ = 550 nm). Such strong NR emission indicates that NR is in a hydrophobic environment since it is encapsulated by the self-assemblies. Upon light irradiation, an abrupt decrease on the initial NR emission was observed in **AcC_{11}Cou-P5N10** due to a migration of NR to a non-hydrophobic environment. This fact can be explained by a complete NR release from the self-assemblies to the aqueous media. In contrast, **Acd_1C_{11}Cou-P5N10** showed a gradual decrease of NR emission, suggesting a more controlled light-induced release of encapsulated molecules (Fig. 10).

Conclusions

In conclusion, we have developed an easy and reliable method to functionalize pillar[5]arene macrocycles through ionic interactions. This approach leads to new ionic materials with promising properties as ion-conductors or drug delivery systems. In the bulk, the ionic pillar[5]arenes self-organize into liquid crystal phases with good proton conductivity. Due to the newly amphiphilic character generated by the ionic moieties, these ionic pillar[5]arenes also self-assemble in water resulting in several nanostructures (*e.g.*, spherical or cylindrical micelles, vesicles, solid nanospheres, or nanotubes) that can encapsulate Nile Red, as a model hydrophobic drug. Additionally, the introduction of coumarin units in the chemical structure of some of our ionic pillar[5]arene leads to nanostructured materials with

photo-responsive properties. Specifically, we demonstrate that coumarin photodimerization can be employed to fabricate mechanical stable proton-conductive liquid crystal materials, as well as to obtain photo-responsive nanocarriers with light-induced release of encapsulated molecules.

Conflicts of interest

There are no conflicts to declare.

Acknowledgements

This work was financially supported by the Spanish projects PGC2018-097583-B-I00, PID2021-122882NB-I00, MCIN/AEI/10.13039/501100011033/ and by "ERDF A way of making Europe", the Gobierno de Aragón-FSE (E47_23R-research group). A. C. acknowledges grant RYC2021-031154-I funded by MICINN/AEI/FEDER/EU-NextGenerationEU. The authors would like to acknowledge the Laboratorio de Microscopias Avanzadas-LMA (Instituto de Nanociencia y Materiales de Aragón-Universidad de Zaragoza), Servicio General de Apoyo a la Investigación-SAI (Universidad de Zaragoza), and Servicios Científico-Técnicos of CEQMA (CSIC-Universidad de Zaragoza) for their support.

References

1 S. Pan, M. Ni, B. Mu, Q. Li, X.-Y. Hu, C. Lin, D. Chen and L. Wang, Well-Defined Pillararene-Based Azobenzene Liquid Crystalline Photoresponsive Materials and Their Thin Films with Photomodulated Surfaces, *Adv. Funct. Mater.*, 2015, **25**, 3571.
2 S. Fa, M. Mizobata, S. Nagano, K. Suetsugu, T. Kakuta, T.-A. Yamagishi and T. Ogoshi, Reversible "On/Off" Chiral Amplification of Pillar[5]arene Assemblies by Dual External Stimuli, *ACS Nano*, 2021, **15**(10), 16794–16801.
3 V. S. Sharma, V. K. Vishwakarma, P. S. Shrivastav, A. A. Sudhakar, A. S. Sharma and P. A. Shah, Calixarene Functionalized Supramolecular Liquid Crystals and Their Diverse Applications, *ACS Omega*, 2022, **7**, 45752–45796.
4 X. Li, B. Li, L. Chen, J. Hu, C. Wen, Q. Zheng, L. Wu, H. Zeng, B. Gong and L. Yuan, Liquid-crystalline mesogens based on cyclo[6]aramides: distinctive phase transitions in response to macrocyclic host–guest interactions, *Angew. Chem., Int. Ed.*, 2015, **54**, 11147–11152.
5 S.-I. Kawano, M. Kato, S. Soumiya, M. Nakaya, J. Onoe and K. Tanaka, Columnar Liquid Crystals from a Giant Macrocycle Mesogen, *Angew. Chem., Int. Ed.*, 2018, **57**, 167–171.
6 L. Chen, Y. Cai, W. Feng and L. Yuan, Pillararenes as macrocyclic hosts: a rising star in metal ion separation, *Chem. Commun.*, 2019, **55**, 7883–7898.
7 X.-Y. Hu, K. Jia, Y. Cao, Y. Li, S. Qin, F. Zhou, C. Lin, D. Zang and L. Wang, Dual Photo- and pH-Responsive Supramolecular Nanocarriers Based on Water-Soluble Pillar[6]arene and Different Azobenzene Derivatives for Intracellular Anticancer Drug Delivery, *Chem. Eur. J.*, 2015, **21**, 1208–1220.
8 R. Wang, Y. Sun, F. Zhang, M. Song, D. Tian and H. Li, Temperature-Sensitive Artificial Channels through Pillar[5]arene-based Host–Guest Interactions, *Angew. Chem., Int. Ed.*, 2017, **56**, 5294–5298.
9 T. Ogoshi, T. Kakuta and T.-A. Yamagishi, Applications of Pillar[n]arene-Based Supramolecular Assemblies, *Angew. Chem., Int. Ed.*, 2019, **58**, 2197–2206.
10 I. Nierengarten, S. Guerra, J.-F. Nierengarten and R. Deschenaux, Building liquid crystals from the 5-fold symmetrical pillar[5]arene core, *Chem. Commun.*, 2012, **48**, 8072–8074.
11 A. Concellón, P. Romero, M. Marcos, J. Barberá, C. Sánchez-Somolinos, M. Mizobata, T. Ogoshi, J. L. Serrano and J. Del Barrio, Coumarin Containing Pillar[5]arenes as Multifuctional Liquid Crystal Macrocycles, *J. Org. Chem.*, 2020, **85**, 8944–8951.
12 I. Nierengarten, S. Guerra, M. Holler, L. Karmazin-Brelot, J. Barberá, R. Deschenaux and J.-F. Nierengarten, Macrocyclic Effects in the Mesomorphic Properties of Liquid-Crystalline Pillar[5]- and Pillar[6]arenes, *Eur. J. Org. Chem.*, 2013, 3675–3684.
13 I. Nierengarten, S. Guerra, H. B. Aziza, M. Holler, R. Abidi, J. Barberá, R. Deschenaux and J.-F. Nierengarten, Piling Up Pillar[5]arenes To Self-Assemble Nanotubes, *Chem. – Eur. J.*, 2016, **22**, 6185–6189.
14 S. Fa, M. Mizobata, S. Nagano, K. Suetsugu, T. Kakuta, T.-A. Yamagishi and T. Ogoshi, Reversible "On/Off" Chiral Amplification of Pillar[5]arene Assemblies by Dual External Stimuli, *ACS Nano*, 2021, **15**, 16794–16801.
15 C. F. J. Faul and M. Antonietti, Ionic Self-Assembly: Facile Synthesis of Supramolecular Materials, *Adv. Mater.*, 2003, **15**, 673–683.
16 C. F. J. Faul, Ionic Self-Assembly for Functional Hierarchical Nanostructured Materials, *Acc. Chem. Res.*, 2014, **47**, 3428–3438.
17 A. Concellón and V. Iguarbe, in *Supramolecular Assemblies Based on Electrostatic Interactions*, ed. M. A. Aboudzadeh, A. Frontera, Springer International Publishing, Cham, 2022, p. 85.
18 S. Hernández-Ainsa, M. Marcos and J. L. Serrano, in *Handbook of Liquid Crystals*, ed. J. W. Goodby, P. J. Collings, T. Kato, C. Tschierske, H. Gleeson and P. Raynes, Wiley-VCH Verlag GmbH & Co. KGaA, 2014, vol. 7, p. 259.
19 M. Marcos, R. Martín- Rapún, A. Omenat and J. L. Serrano, Highly congested liquid crystal structures: dendrimers, dendrons, dendronized and hyperbranched polymers, *Chem. Soc. Rev.*, 2007, **36**, 1889–1901.
20 A. Concellón, M. San Anselmo, S. Hernández-Ainsa, P. Romero, M. Marcos and J. L. Serrano, Micellar Nanocarriers from Dendritic Macromolecules Containing Fluorescent Coumarin Moieties, *Polymers*, 2020, **12**, 2872.
21 M. Cano, A. Sánchez-Ferrer, J. L. Serrano, N. Gimeno and B. Ros, Supramolecular Architectures from Bent-Core Dendritic Molecules, *Angew. Chem., Int. Ed.*, 2014, **53**, 13449–13453.
22 S. Hernández-Ainsa, J. Barberá, M. Marcos and J. L. Serrano, Nanoobjects Coming From Mesomorphic PAMAM Ionic derivatives, *Soft Matter*, 2011, **7**, 2560–2568.
23 A. Concellón, A. P. H. J. Schenning, P. Romero, M. Marcos and J. L. Serrano, Size-Selective Adsorption in Nanoporous

Polymers from Coumarin Photo-Cross-Linked Columnar Liquid Crystals, *Macromolecules*, 2018, **51**, 2349–2358.

24 A. Concellón, T. Liang, A. P. H. J. Schenning, J. L. Serrano, P. Romero and M. Marcos, Proton-conductive materials formed by coumarin photocrosslinked ionic liquid crystal dendrimers, *J. Matter. Chem. C*, 2018, **6**, 1000–1007.

25 C. Mertesdorf and H. Ringsdorf, Self-organization of substituted azacrowns based on their discoid and amphiphilic nature, *Liq. Cryst.*, 1989, **5**, 1757–1772.

26 C. Lin, H. Ringsdorf, M. Ebert, R. Kleppinger and J. H. Wendorff, Structural variations of liquid crystalline polymers with phasmidic-type mesogens, *Liq. Cryst.*, 1989, **5**, 1841–1847.

27 A. Concellón, M. Marcos, P. Romero, J. L. Serrano, R. Termine and A. Golemme, Not Only Columns: High Hole Mobility in a Discotic Nematic Mesophase Formed by Metal-Containing Porphyrin-Core Dendrimers, *Angew. Chem., Int. Ed.*, 2017, **129**, 1279–1283.

28 Y. Sun, F. Zhang, J. Quan, F. Zhu, W. Hong, J. Ma, H. Pang, Y. Sun, D. Tian and H. Li, A biomimetic chiral-driven ionic gate constructed by pillar[6]arene-based host–guest systems, *Nat. Commun.*, 2018, **9**, 2617.

29 A. Pérez, D. de Saá, A. Ballesteros, J. L. Serrano, T. Sierra and P. Romero, NMR Spectroscopic Study of the Self-Aggregation of 3-Hexen-1,5-diyne Derivatives, *Chem. – Eur. J.*, 2013, **19**, 10271–10279.

30 H. Cabral, K. Miyata, K. Osada and K. Kataoka, Block Copolymer Micelles in Nanomedicine Applications, *Chem. Rev.*, 2018, **118**, 6844–6892.

31 M. Abad, M. Nardi, L. Oriol, M. Piñol and E. Blasco, Aqueous seeded RAFT polymerization for the preparation of self-assemblies containing nucleobase analogues, *Polym. Chem.*, 2023, **14**, 71–80.

32 L. Rui, L. Liu, Y. Wang, Y. Gao and W. Zhang, Orthogonal Approach to Construct Cell-Like Vesicles via Pillar[5]arene-Based Amphiphilic Supramolecular Polymers, *ACS Macro Lett.*, 2016, **5**, 112–117.

33 L. Shao, B. Hua, J. Yang and G. Yu, Pillar[7]arene-based host–guest complex in water: dual-responsiveness and application in controllable self-assembly, *RSC Adv.*, 2016, **6**, 60029–60033.

34 G. Yu, W. Yu, Z. Mao, C. Gao and F. Huang, A pillararene-based ternary drug-delivery system with photocontrolled anticancer drug release, *Small*, 2015, **11**, 919–925.

35 D. Wang, T. Zhang, B. Wu, C. Ye, Z. Wei, Z. Cao and G. Wang, Reversibly Photoswitchable Dual-Color Fluorescence and Controlled Release Properties of Polymeric Nanoparticles, *Macromolecules*, 2019, **52**, 7130–7136.

36 Y. C. Gong, X. Y. Xiong, X. J. Ge, Z. L. Li and Y. P. Li, Effect of the Folate Ligand Density on the Targeting Property of Folated-Conjugated Polymeric Nanoparticles, *Macromol. Biosci.*, 2019, **19**, 1800348.

37 A. Concellón, E. Blasco, A. Martínez-Felipe, J. C. Martínez, I. Šics, T. A. Ezquerra, A. Nogales, M. Piñol and L. Oriol, Light-Responsive Self-Assembled Materials by Supramolecular Post-Functionalization via Hydrogen Bonding of Amphiphilic Block Copolymers, *Macromolecules*, 2016, **49**, 7825–7836.